# Spreading depolarizations : the missing link between mirgraine and stroke

Ayata, C.

# CHAPTER 3

## IMPACT OF SPREADING DEPRESSION SUSCEPTIBILITY ON STROKE OUTCOME

# CHAPTER 3A

## MIGRAINE MUTATIONS INCREASE STROKE VULNERABILITY BY FACILITATING ISCHEMIC DEPOLARIZATIONS

Katharina Eikermann-Haerter,[1] Jeong Hyun Lee,[1] Izumi Yuzawa,[1] Christina H. Liu,[2] Zhipeng Zhou,[1,4] Hwa Kyoung Shin,[1,5] Yi Zheng,[1] Tao Qin,[1] Tobias Kurth,[6,7] Christian Waeber,[1] Michel D. Ferrari,[8] Arn M.J.M. van den Maagdenberg,[8,9] Michael A. Moskowitz,[1] and Cenk Ayata[1,3]

[1]Stroke and Neurovascular Regulation Laboratory, Department of Radiology, Athinoula A. Martinos Center for Biomedical Imaging and [2]Transcript Imaging and NeuroRepair Laboratory, Division of Neuroradiology, and [3]Stroke Service and Neuroscience Intensive Care Unit, Department of Neurology, Massachusetts General Hospital, Harvard Medical School, Charlestown, Massachusetts, USA; [4]Department of Radiology, Affiliated Hospital of Guilin Medical College, Guilin, China; [5]Division of Meridian and Structural Medicine, School of Korean Medicine, Pusan National University, Yangsan, Republic of Korea; [6]INSERM Unit 708, Neuroepidemiology, University of Bordeaux, Bordeaux, France; [7]Division of Preventive Medicine, Brigham and Women's Hospital, Harvard Medical School, Boston, Massachusetts, USA; and [8]Departments of Neurology and [9]Human Genetics, Leiden University Medical Center, Leiden, the Netherlands.

*Circulation 2012; 125: 335-345.*

## ABSTRACT

**Background**: Migraine is an independent risk factor for stroke. Mechanisms underlying this association are unclear. Familial hemiplegic migraine (FHM), a migraine subtype that also carries an increased stroke risk, is a useful model for common migraine phenotypes because of shared aura and headache features, trigger factors, and underlying glutamatergic mechanisms.

**Methods and Results**: Here, we show that FHM type 1 (FHM1) mutations in $Ca_V2.1$ voltage-gated $Ca^{2+}$ channels render the brain more vulnerable to ischemic stroke. Compared with wild-type mice, 2 FHM1 mutant mouse strains developed earlier onset of anoxic depolarization and more frequent peri-infarct depolarizations associated with rapid expansion of infarct core on diffusion-weighted magnetic resonance imaging and larger perfusion deficits on laser speckle flowmetry. Cerebral blood flow required for tissue survival was higher in the mutants, leading to infarction with milder ischemia. As a result, mutants developed larger infarcts and worse neurological outcomes after stroke, which were selectively attenuated by a glutamate receptor antagonist.

**Conclusions**: We propose that enhanced susceptibility to ischemic depolarizations akin to spreading depression predisposes migraineurs to infarction during mild ischemic events, thereby increasing the stroke risk.

## INTRODUCTION

Migraine is the most common neurological condition affecting young to middle-age adults. Up to one third of migraineurs experience transient neurological symptoms called aura. Migraine, particularly with aura, is associated with increased stroke risk both during and between attacks, especially in women.[1-4] The biological basis for this association is unknown. Stroke risk is also increased in familial hemiplegic migraine (FHM), a monogenic migraine subtype with hemiplegic auras in addition to the common aura forms.[5] FHM is a useful model for common migraine with aura because of shared clinical features and trigger factors, female preponderance, and because two thirds of FHM patients and their first-degree relatives also have attacks of common migraine with or without aura.[6,7] Neuronal network hyperexcitability and enhanced glutamate release have been implicated in both FHM and common forms of migraine.[8]

FHM type 1 (FHM1) is caused by mutations in the *CACNA1A* gene, which encodes the pore-forming $\alpha_{1A}$ subunit of neuronal $Ca_V2.1$ voltage-gated $Ca^{2+}$ channels.[9] Presynaptic $Ca_V2.1$ channels are major regulators of excitatory neurotransmitter release. FHM1 mutant channels open with smaller depolarizations and stay open longer,[10] which augments presynaptic $Ca^{2+}$ entry and glutamate release, thereby enhancing brain excitability.[11] Transgenic mice expressing the human R192Q or S218L FHM1 mutation show an increased susceptibility to spreading depression, the electrophysiological substrate for migraine, and display characteristic clinical features of FHM such as transient hemiplegia.[12-14] Glutamatergic mechanisms and hyperexcitability also have been implicated in the pathogenesis of common forms of migraine.[15,16] Genetic support for this link was recently obtained in a genome-wide association study identifying the astrocyte elevated gene 1 (*AEG1*), encoding a regulator of glial glutamate transporter EAAT2, as the first migraine gene.[16]

Glutamate excitotoxicity also plays a pivotal role in the pathogenesis of stroke. Therefore, we hypothesized that genetic mutations conferring cerebral hyperexcitability and migraine susceptibility increase the vulnerability to ischemic stroke, as 1 mechanism to explain the migraine-stroke association. We tested this hypothesis using $Ca_V2.1$ S218L and R192Q transgenic mouse models of FHM1. The results reveal electrophysiological and hemodynamic mechanisms that accelerate hyperacute stroke evolution and worsen ischemic outcome in FHM1 mutants and suggest a pivotal role for enhanced glutamatergic transmission in increasing the vulnerability to ischemic stroke in susceptible migraineurs.

## METHODS

**Experimental Animals.** Experimental procedures were approved by the institutional review boards. A total of 267 male and female mice were used. Transgenic knock-in *Cacna1a* migraine mouse models homozygous (HOM) or heterozygous (HET) for

R192Q or S218L FHM1 mutations were generated by a gene targeting approach.[14] The R192Q mutant strain was compared with C57BL6/J, backcrossed for 10 generations. The S218L mutants were compared with their wild-type (WT) littermates. Because stroke risk is highest in young adult migraineurs, mice were studied between 2 and 6 months of age. All experiments were carried out by blinded investigators, and confirmatory genotyping was done.

**Systemic Physiological Monitoring.** Arterial pH, $PO_2$, $PCO_2$, and blood pressure were measured via a femoral artery catheter under isoflurane anesthesia (2.5% induction, 1.5% maintenance, in 70% $N_2O$ and 30% $O_2$; Supplemental Table 1). Rectal temperature was controlled at 37°C during ischemia, and intermittent monitoring was continued for 6 hours in a subset of mice.

**Transient Filament Occlusion of the Middle Cerebral Artery.** A nylon monofilament was inserted into the internal carotid artery via the external carotid artery followed by reperfusion after 30 or 60 minutes under isoflurane anesthesia (2.5% induction, 1.5% maintenance, in 70% $N_2O$ and 30% $O_2$) and laser Doppler monitoring. Mice were placed in a temperature-controlled incubator with easy access to food and water. Neurological outcomes were scored 24 hours after reperfusion with a 5-point scale: 0, normal; 1, forepaw monoparesis; 2, circling to left; 3, falling to left; 4, no spontaneous walking and depressed consciousness; and 5, death. Infarct volume was calculated by integrating the infarct area in ten 1-mm-thick 2,3,5-triphenyltetrazolium chloride (TTC)-stained coronal sections. Infarct volumes were calculated by subtracting the volume of ipsilateral noninfarcted tissue from the contralateral hemisphere. Ischemic swelling volumes were calculated by subtracting the volume of contralateral hemisphere from the volume of ipsilateral hemisphere. Glutamatergic mechanisms were tested by administering MK-801 (1 mg/kg IP; Sigma, St Louis, MO) 15 minutes before filament occlusion of the middle cerebral artery (fMCAO).

**Magnetic Resonance Imaging.** Apparent diffusion coefficient maps were acquired under isoflurane anesthesia with a 9.4-T magnetic resonance imaging (MRI) scanner (Bruker Biospin, Inc, Billerica, MA) 30 and 60 minutes after fMCAO (repetition time/echo time, 3000/27 milliseconds; b, 154 and 1294 s/mm$^2$; in-plane resolution, 180 x 180 μm$^2$; slice thickness, 1 mm; number of averaging, 8). Means and SDs of the apparent diffusion coefficient in the cortex, striatum, hippocampus, and thalamus were extracted from the normal hemisphere, and thresholds were defined as mean minus 2 SDs to calculate lesion volumes. Normal systemic physiological parameters were confirmed under simulated MRI conditions in a separate group of mice (not shown).

**Electrophysiological Recordings.** After fMCAO, isoflurane-anesthetized mice were intubated and ventilated, and the femoral artery was catheterized for blood pressure

and blood gas monitoring. Two intracortical glass micropipettes were placed, and extracellular recordings (depth, 250 μm) were started within 15 minutes after the onset of ischemia and continued for ≈2 hours.

**Receptor Autoradiography.** The density and distribution of glutamate and GABAA receptors and glutamate reuptake sites were assessed on 10-μm frozen sections with tritium-sensitive storage phosphor screens (GE Healthcare) as described.[17]

**Laser Speckle Flowmetry.** Spontaneously breathing mice (S218L HOM) were anesthetized with isoflurane as above, and the femoral artery was catheterized for blood pressure and gas measurements. Mice were placed in a stereotaxic frame; a temporal burr hole (2-mm diameter) was drilled above the zygomatic arch; and the distal middle cerebral artery was occluded with a microvascular clip for 60 minutes. Cortical perfusion was imaged during distal middle cerebral artery occlusion with laser speckle flowmetry through intact skull.[18] Cerebral blood flow (CBF) changes were calculated for each pixel relative to the preischemic baseline, and the area of cortex with residual CBF ≤30% was determined by thresholding. Neurological outcomes and infarcts were assessed 48 hours later as described above. In addition, the CBF threshold for tissue viability was estimated by superimposing the images of CBF and infarct. In the R192Q HOM strain, mice were intubated and ventilated to ensure normal arterial blood gas values, precluding survival for neurological and infarct assessment in this strain.

**Anatomic Analysis of the Circle of Willis and Pial Collaterals.** Mice were transcardially perfused with carbon black. The diameter of cerebral arteries, patency of the posterior communicating artery, and number of pial arterial anastomoses between the anterior, posterior, and middle cerebral arteries and their distance from midline were determined.

**Absolute Resting CBF.** Mice were anesthetized with α-chloralose (50 mg/kg) and ventilated. The femoral artery and external jugular vein were cannulated. Arterial blood was withdrawn continuously (0.3 mL/min). *N*-isopropyl-[methyl-1,3-$^{14}$C]-p-iodoamphetamine (1 μCi) was injected in 0.1 mL saline over 10 seconds. Twenty seconds after injection, the animal was decapitated, and the blood withdrawal was terminated simultaneously. The brain was removed, frozen, and dissected. CBF was calculated from the radioactivity in tissue and blood measured by liquid scintillation spectrometry.

**Statistical Analysis.** Data were analyzed with SPSS (version 11.0) and are presented as mean ± SE or median and interquartile range. We used the $\chi^2$ test to compare proportions, ANOVA to compare mean values of continuous measures according to genotypes, and general linear models for repeated measures to compare mean values over time according to genotypes. Comparisons of disability scores were performed

by the use of nonparametric rank tests; cumulative peri-infarct depolarization (PID) incidence was compared by the log-rank test; and PID frequency versus the area of CBF deficit was assessed by the Pearson correlation test. *P* values are 2 tailed, and values of $P<0.05$ were considered statistically significant.

## RESULTS

**Enhanced Susceptibility to Anoxic and Peri-Infarct Depolarizations.** Anoxic depolarization is characterized by a sudden loss of membrane ionic gradients, uncontrolled glutamate release, and cell swelling, triggered by the failure of $Na^+/K^+$ ATPase under ischemic conditions. We found significantly earlier onset of anoxic depolarization in FHM1 mutants after fMCAO by monitoring its vasoconstrictive effect on cerebral vasculature as previously described (Figure 1A and 1B).[18,19] Importantly, the magnitude of CBF reduction in the ischemic core did not differ among groups in this fMCAO model, eliminating the possibility that faster anoxic depolarization rates were due to more severe ischemia (residual CBF, 10% to 17% of baseline in both S218L and R192Q; $P=0.634$ and 0.599, respectively; data not shown).

PIDs are recurrent propagating depolarization waves akin to spreading depression that exacerbate the metabolic mismatch in penumbra and promote infarct growth during hyperacute stroke.[18-21] We reasoned that FHM1 mutations that enhance spreading depression susceptibility[13] might also facilitate the occurrence of PIDs. Using intracortical microelectrode recordings during fMCAO, we indeed found a 2-fold increase in the frequency of PIDs in mutants over WT (5.3±1.3 versus 2.6±0.3 PIDs per hour; $P=0.028$; Figure 1C–1F). In the mutants, PIDs sometimes occurred in clusters, possibly reflecting circling around the ischemic core (see below),[22] but otherwise did not differ from WT in terms of durations and amplitudes (not shown). Together, these data suggest that genetically enhanced susceptibility to spreading depression[11-14] facilitates the occurrence of anoxic depolarization and PIDs during acute stroke as a novel mechanism to explain increased stroke vulnerability in migraineurs.

**Rapid Growth of Hyperacute Ischemic Core on MRI.** To assess whether enhanced susceptibility to anoxic depolarization and PIDs accelerates the hyperacute stroke evolution in FHM1 mutants, we performed serial diffusion-weighted MRI during fMCAO. Reduced apparent diffusion coefficient values on diffusion-weighted MRI reflect anoxic depolarization, loss of transmembrane ionic gradients, and cell swelling (ie, ischemic core). We found that the apparent diffusion coefficient lesion volumes expanded more rapidly in FHM1 mutant strains compared with WT controls (Figure 2). Although larger apparent diffusion coefficient lesion volumes were due primarily to more severe cortical involvement, the hyperacute lesion also encompassed the hippocampus and thalamus in S218L mutants.

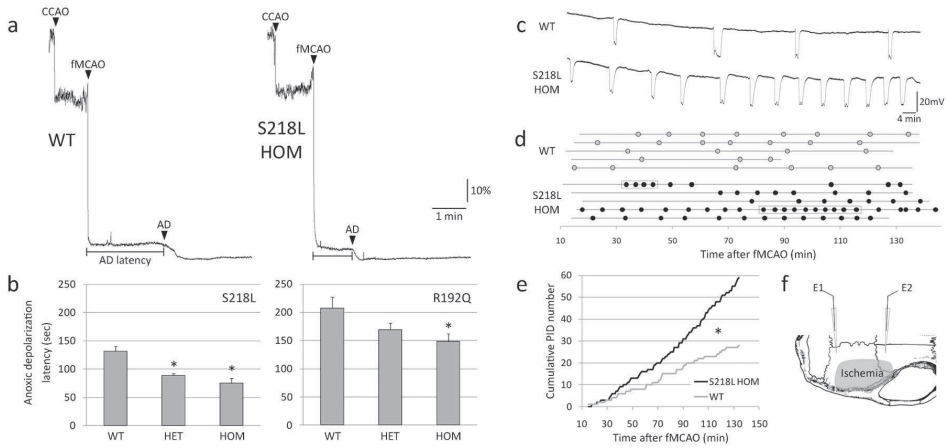


**Figure 1. Faster anoxic depolarization (AD) rates and more frequent peri-infarct depolarizations (PIDs) in FHM1 mutant mice.** (**A**) Representative laser Doppler tracings show cerebral blood flow (CBF) reduction on common carotid artery occlusion (CCAO) followed by filament occlusion of the middle cerebral artery (fMCAO). A further decline in CBF marks the onset of AD and is due to the vasoconstrictive effect of tissue depolarization on ischemic microvasculature.[18] Scale bars: vertical, 10%; horizontal, 1 minute. (**B**) The latency to AD was shorter in S218L and R192Q mutants ($P<0.001$ and $P=0.035$, respectively), with a trend for an allele-dosage effect. *$P<0.05$ vs wild type (WT). (**C**) Representative electrophysiological tracings show more frequent PIDs in S218L homozygous (HOM) vs WT. Scale bars: vertical, 20 mV; horizontal, 4 minutes. (**D**) PIDs (round symbols shown as a function of time) occurred in S218L HOM mice more frequently and sometimes in clusters (rectangular boxes). Horizontal lines indicate the time of onset and end of electrophysiological recordings in each mouse (n=5 each). When the average PID frequency was calculated, these minor differences in recording duration were taken into account. (**E**) Pooled cumulative PID numbers as a function of time after fMCAO was more than doubled in S218L HOM mice (*$P<0.001$; n=5 each). (**F**) Experimental setup showing 2 intracortical glass micropipettes (E1, E2) placed outside the ischemic territory to detect PIDs after fMCAO. Shaded area indicates typical distribution of CBF deficit after fMCAO. HET indicates heterozygous.

**Larger Perfusion Deficit During Hyperacute Stroke.** Ischemic depolarizations compromise residual CBF within the territory supplied by the occluded artery via vasoconstrictive (ie, inverse) neurovascular coupling[18,19] as a major determinant of outcome in cerebral ischemia. Using laser speckle flowmetry, we found larger cortical perfusion deficits after distal middle cerebral artery occlusion in FHM1 mutants (Figure 3A and 3B; only S218L shown), associated with an increased frequency of PIDs (0.9±0.3 versus 4.6±1.2 PIDs per hour in WT and S218L HOM, respectively; Figure 3C) that circled around the hypoperfused core in 38% of S218L mutants but not in the WT (movies I and II in the online-only Data Supplement).[22] In fact, higher PID frequencies were associated with larger cortical CBF deficits (Figure 3D), bigger infarcts (Figure 3E and 3F), and worse neurological outcomes (deficit score, 1 [interquartile range, 1–1] versus 0 [interquartile range, 0–0.25] in S218L HOM and WT mice, respectively; $P=0.019$). These data suggest that ischemic depolarizations adversely influence the

perfusion deficits and exacerbate the metabolic and O2 supply-demand mismatch in FHM1 mutants, in part via vasoconstrictive (ie, inverse) neurovascular coupling as an additional hemodynamic mechanism for infarct growth.[18,19,23]

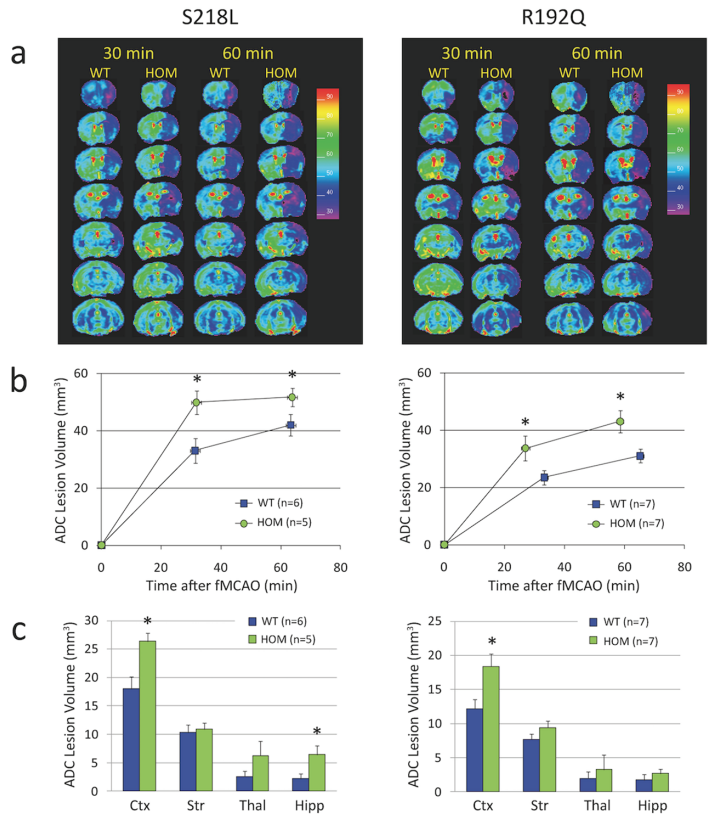


**Figure 2. FHM1 mutant mice show accelerated lesion growth on magnetic resonance imaging (MRI) during hyperacute stroke.** (**A**) Apparent diffusion coefficient (ADC) lesion (ie, ischemic core with restricted water diffusion, purple) was larger on diffusion-weighted MRIs in S218L (left) and R192Q (right) mutants vs wild type (WT) during the hyperacute phase after filament occlusion of the middle cerebral artery (fMCAO). (**B**) ADC lesion volumes shown as a function of time after fMCAO were 40% to 50% larger in S218L and R192Q homozygous (HOM) vs WT as early as 30 minutes after fMCAO, suggesting faster growth of the ischemic core ($P$=0.019 and $P$=0.018, respectively). The difference remained significant at 60 minutes. Vertical and horizontal error bars reflect the SEs for total ADC lesion volume and timing of MRI scans, respectively. (**C**) Thirty minutes after stroke onset, enlarged ADC lesion volumes in S218L HOM and R192Q HOM were due primarily to more severe cortical involvement ($P$=0.015 and $P$=0.023, respectively), although S218L HOM mutants also showed hyperacute ADC changes in the hippocampus and thalamus ($P$=0.018 and $P$=0.117, respectively). Of note, the average regional ADC values in the center of ischemic core did not significantly differ between FHM1 mutants and their WT controls, suggesting that cytotoxic cell swelling is complete in ischemic core in all groups (60±7% versus 56±6% in R192Q WT and HOM, and 57±5% versus 57±6% of contralateral hemisphere in S218L WT and HOM, respectively, 60 minutes after stroke onset). *$P$<0.05 vs WT. Ctx, cortex; Str, striatum; Thal, thalamus; Hipp, hippocampus.

Importantly, we found no difference in absolute resting CBF values between WT and R192Q HOM mice in the cortex, striatum, and cerebellum using the [$^{14}$C] iodoamphetamine method (Supplemental Table 2), indicating that differences in

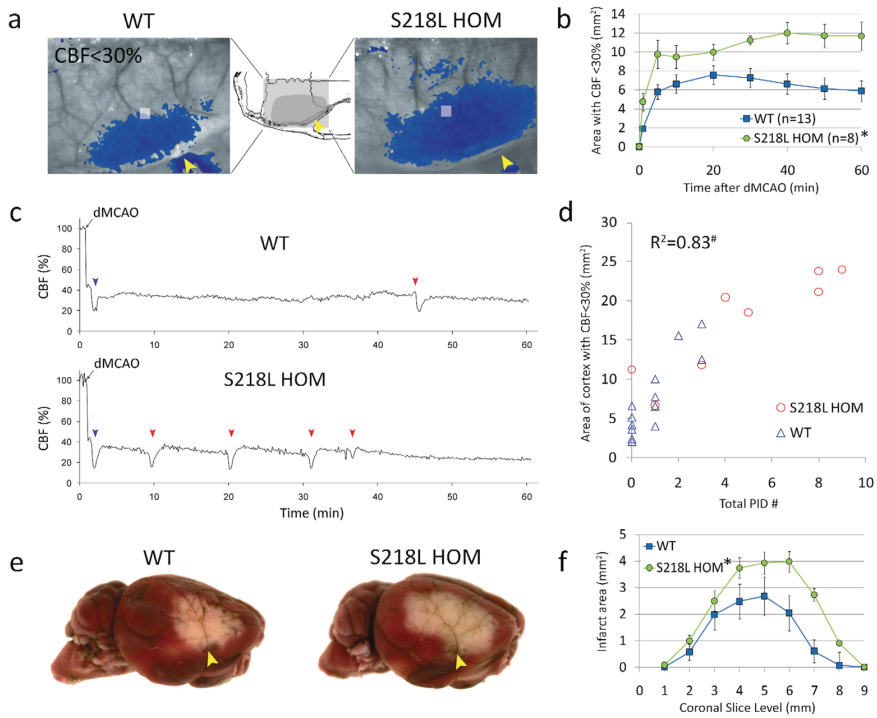


**Figure 3. FHM1 mutant mice develop larger areas of cerebral blood flow (CBF) deficit during distal middle cerebral artery occlusion (dMCAO) because of increased susceptibility to ischemic depolarizations.** (**A**) Representative laser speckle contrast images show the area of cortex with ≤30% residual CBF vs preischemic baseline (blue pixels) 60 minutes after dMCAO in wild-type (WT) and S218L homozygous (HOM) mice. Similar data were obtained with the R192Q strain (n=6 mutant and 6 WT; data not shown). Imaging was performed over the right hemisphere (light gray–shaded rectangle in the inset) through intact skull. Arrowheads indicate clip occlusion. (**B**) The area of CBF deficit expanded rapidly in S218L HOM throughout the 60-minute dMCAO (*$P$=0.004). (**C**) Representative tracings show cortical blood flow reductions in penumbra (measured within the gray squares shown in A) after dMCAO. Anoxic depolarization triggers the first peri-infarct depolarization (PID; blue arrowheads), marking a second abrupt reduction in perfusion. Each subsequent PID (red arrowheads) causes a characteristic blood flow transient. (**D**) The frequency of PIDs was higher in S218L HOM and correlated with the area of hypoperfused cortex 60 minutes after dMCAO (#$P$<0.001). Each symbol represents the PID frequency in individual mice. (**E**) Representative 2,3,5-triphenyltetrazolium chloride–stained whole brains show enlarged infarcts in S218L HOM 48 hours after 60 minutes of dMCAO. (**F**) The area of infarcts in 1-mm-thick coronal slices (0=anterior, 9=posterior) were larger in S218L HOM vs WT (*$P$=0.016, S218L HOM vs WT for infarct areas). Integrated total infarct volumes were also larger in the mutants (19±3 versus 11±2 mm$^3$, respectively; $P$=0.008).

preischemic resting CBF did not influence our measurements. We also confirmed this in WT and S218L HOM mice under isoflurane anesthesia using the correlation time values obtained by laser speckle imaging, which allow direct comparison of resting CBF among groups of mice (data not shown).[24,25] Moreover, the incidence of incomplete circle of Willis, the diameter of its major branches, and the number and location of pial arterial anastomoses did not differ between WT and S218L HOM mice, suggesting that developmental differences in cerebrovascular anatomy did not contribute to worse perfusion deficits in the mutant mice (Supplemental Figure 1 and Supplemental Table 3).

**Higher CBF Threshold for Tissue Survival.** To determine the critical tissue perfusion level below which infarction ensued (ie, viability threshold), we calculated the regional CBF at the infarct margin by spatially coregistering the laser speckle perfusion map during distal middle cerebral artery occlusion with the infarct that developed 48 hours later (Figure 4). We found that cortical tissue in S218L HOM mutants required a higher CBF level for survival compared with WT mice (42±3% versus 35±2% of baseline CBF, respectively; $P$=0.048). These data underscore the importance of parenchymal mechanisms such as neuronal hyperexcitability and ischemic depolarizations as the main cause for increased vulnerability to ischemic stroke in FHM1 mutants independently of the severity of CBF deficit.

**Worse Stroke Outcomes.** Enhanced susceptibility to anoxic depolarization and PID and accelerated hyperacute infarct growth with more severe CBF deficits translated into worse stroke outcomes in FHM1 mutants. Transient fMCAO for 1 hour produced larger infarcts in both S218L and R192Q mutant mice compared with their WT controls (Figure 5A). Larger infarcts reflected predominantly more severe cortical involvement in both mutants (>70% of total infarct volume); however, the incidence of hippocampal or thalamic infarction also tended to be higher in the S218L mutant (present in 33% of S218L HET mice compared with 13% of WT; $P$=0.1; data not shown), consistent with a higher incidence of subcortical infarction observed on MRI in this strain (see above). Functional outcomes, assessed with a combined death and neurological disability score as a clinically relevant end point, were worse in mutants compared with WT (Table 1). Indeed, the mortality rate was significantly higher in the S218L mutants, reaching 100% in the HOM within 24 hours after stroke onset (Supplemental Figure 2a). The timing of death after stroke was variable (12±3 hours after stroke onset) and was not associated with overt seizure activity. Immediate postmortem examination revealed 2-fold larger infarcts in S218L HOM compared with WT mice euthanized at the same time point of death of each mutant after 60 minutes of fMCAO (95±15 versus 44±7 mm3, respectively; n=5 and 4; $P$=0.031), suggesting that selection bias resulting from high mortality in the mutants diminished the strain differences in outcome.

These data were excluded from the overall comparisons among genotypes (Figure 5) because of variable time of death. Ischemic brain swelling tended to be more severe in the mutants in proportion to the actual infarct volume and might have contributed to the high mortality in the S218L mutants.

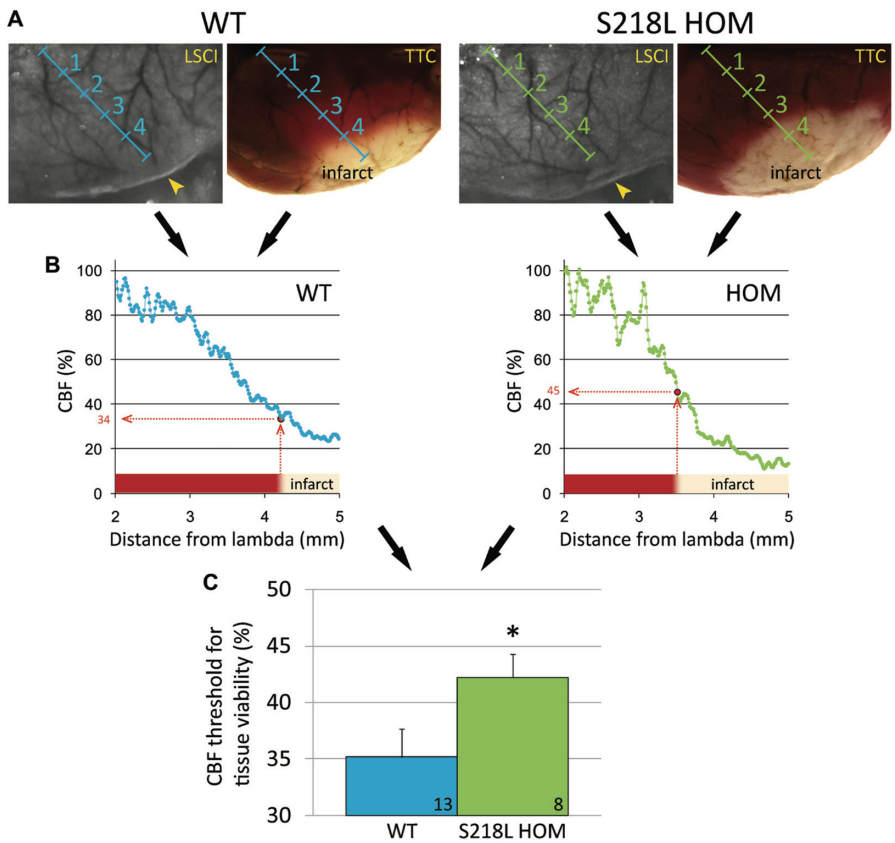


**Figure 4. Elevated blood flow threshold for tissue survival in FHM1 mutant mice.** (**A**) Representative laser speckle contrast images (LSCI) during distal middle cerebral artery occlusion (dMCAO; left) and 2,3,5-triphenyltetrazolium chloride (TTC)-stained brain showing the infarct 48 hours after 60 minutes of dMCAO (right) are shown for wild-type (WT) and S218L homozygous (HOM) mice. Imaging field was positioned as shown in Figure 3A. Images were spatially coregistered through the use of surface landmarks. Line profiles (blue and green oblique lines, labeled in mm) were drawn between lambda and the clip occluding the middle cerebral artery branch (yellow arrowheads). (**B**) For each animal, cortical blood flow (CBF) was plotted along these line profiles as a function of distance from lambda using laser speckle images, and the blood flow level corresponding to the infarct edge was determined (red dotted lines). This value represented the CBF threshold for viability, below which the tissue infarcted in each mouse. (**C**) The average viability threshold was significantly higher in S218L HOM mutants vs WT controls ($P$=0.048), indicating that FHM1 mutant brains are more vulnerable to ischemia and require higher blood flow to survive. The numbers of mice are shown on each bar. *$P$<0.05 vs WT.

| | 60-min fMCAO* | | | 60-min fMCAO+ MK-801†‡ | | 30-min fMCAO§ | | | | |
|---|---|---|---|---|---|---|---|---|---|---|
| | Male WT | Male HET | Male HOM | Male WT | Male HET | Male WT | Male HET | Male HOM | Female WT | Female HET |
| n | 9 | 23 | 8 | 9 | 10 | 9 | 5 | 4 | 6 | 8 |
| Mortality, % | 11 | 35 | 100 | 0 | 10 | 0 | 0 | 75 | 0 | 0 |
| Functional outcome score | 2 (2–3) | 3 (2–5) | 5 (5–5) | 2 (1–2) | 2 (1–2) | 1 (1–2) | 2 (1–2) | 5 (4–5) | 1 (0.3–1) | 2 (1–2) |

**Table 1. Death and Neurological Disability After Transient Filament Occlusion of the Middle Cerebral Artery in S218L Mutant Mice.** fMCAO indicates filament occlusion of the middle cerebral artery; WT, wild type; HET, heterozygous; and HOM, homozygous. Functional outcome scores are shown as median (interquartile range); 0 best, 5 worst (see Methods for the scoring system). **P*<0.001 and *P*=0.008 for the effect of genotype on mortality and functional outcome score, respectively. †*P*=0.353 and *P*=0.757 for the effect of genotype on mortality and functional outcome score, respectively. ‡*P*=0.303 and *P*=0.315 for the effect of MK-801 on mortality and functional outcome score, respectively, in WT and *P*=0.022 and *P*=0.009, respectively, in the S218L HET compared with the untreated group. §*P*<0.001 and *P*=0.086 for the effect of genotype on mortality and functional outcome score in males, respectively, and *P*=0.02 for the effect of genotype on functional outcome score in females after 30 minutes of fMCAO. In the R192Q mutant strain, the mortality rate was 17%, 0%, and 14% in WT, HET, and HOM, respectively; neurological disability was not studied in this mutant strain.

To mimic transient ischemic attacks and to circumvent the high mortality rate in S218L HOM mice, we subjected this mutant strain to 30 minutes of fMCAO. With a shorter duration of ischemia, we did not detect overt infarcts in 27% of WT mice using TTC staining, whereas all S218L HET and HOM mutant mice developed conspicuous territorial infarcts (*P*=0.077). Selective ischemic changes in scattered neurons were nevertheless present on histological examination of brains without an overt infarct (not shown). Infarct volumes were once again larger in the S218L mutants compared with WT mice (Figure 5B). The volume of subcortical infarction, limited to the striatum in this shorter ischemia model, was also larger in the S218L HET compared with WT mice (17±4 and 5±1 $mm^3$, respectively, in males, *P*=0.002; 16±3 and 4±2 $mm^3$, respectively, in females, *P*=0.013). Despite the shorter ischemia duration, mortality was still high in the S218L HOM mutants (75%), but all HET mutants survived for at least 24 hours and showed a trend for worse functional outcome compared with WT (*P*=0.086; Table 1).

Because classic migraine, sporadic migraine, and FHM are more prevalent in women of reproductive age[5,26-29] and because susceptibility to spreading depression is higher in female FHM1 mutant mice compared with males,[13,30] we also studied female mice and found an even more striking increase in infarct volumes in S218L HET compared with WT (Figure 5B). To assess long-term tissue and neurological outcome (2 weeks) in FHM1 mutants, we subjected female S218L HET and WT mice to 30 minutes of fMCAO. However, we observed >60% mortality in the mutants predominantly between 24 and 96 hours, which precluded outcome comparisons between the mutant and WT strains at this late time point (Supplemental Figure 2b). Together, these data indicate

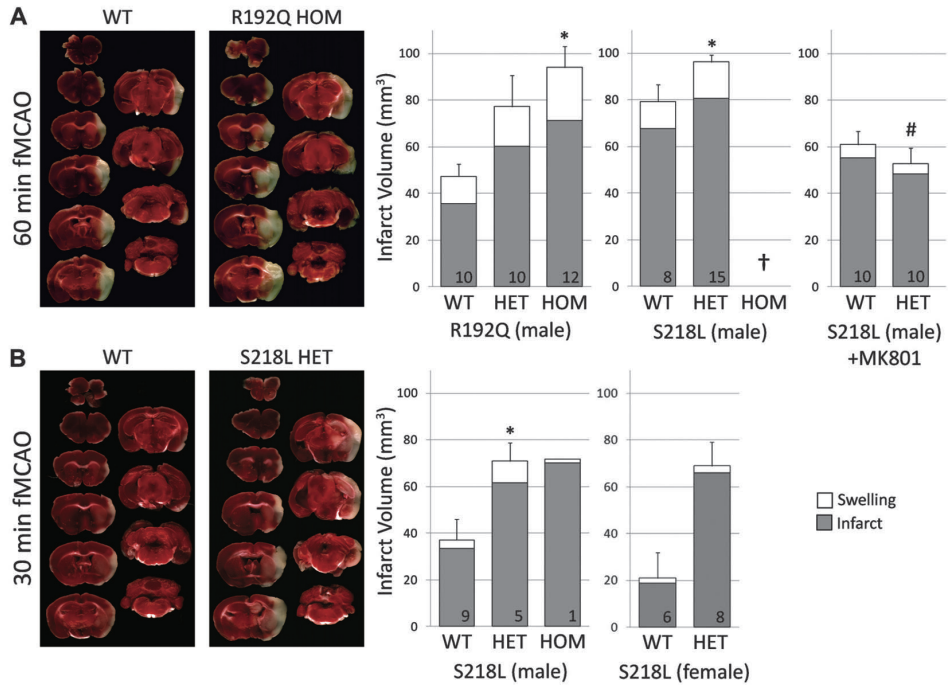


**Figure 5. FHM1 mutant mice develop larger infarcts after experimental stroke selectively attenuated by the *N*-methyl-*D*-aspartate receptor antagonist MK-801.** Left, Representative infarcts (unstained white tissue) 24 hours after filament occlusion of the middle cerebral artery (fMCAO). Right, Infarct and ischemic swelling volumes (gray and white bars, respectively). (**A**) After 60 minutes of fMCAO, infarcts were larger in both R192Q and S218L mutants vs wild type (WT; *P*=0.007 and *P*=0.019, respectively). One of 9 WT, 8 of 23 S218L heterozygous (HET), and all 8 S218L homozygous (HOM; †) mice died within 24 hours (Table 1) and were excluded from infarct volume analysis. Because genetic backgrounds and infarct volumes differed significantly between WT controls of the 2 mutant strains, we did not directly compare S218L and R192Q mutants in this study. MK-801 (1 mg/kg IP 15 minutes before fMCAO) significantly reduced infarct volume in the S218L HET mutants (*P*<0.001 vs untreated S218L HET shown in A) but not in the WT (*P*=0.061 vs untreated WT shown in A). Therefore, MK-801 was more efficacious in FHM1 mutants (*P*=0.026 for infarct reduction by MK-801 between WT and FHM1 mutants). As a result, after MK-801, infarct and swelling volumes were comparable between WT and S218L HET mice (*P*=0.367), as were neurological outcomes (Table 1). (**B**) Thirty minutes of fMCAO also resulted in larger infarcts in male and female S218L mutants vs WT (*P*=0.028). Despite shorter ischemia, 3 of 4 S218L HOM mutants died within 24 hours and were again excluded from infarct volume analysis; the data from the only surviving HOM mutant are shown. There was no mortality in the WT and HET groups after 30 minutes of fMCAO. The numbers of mice are shown on each bar. SE bars and *P* values refer to total volume (ie, infarct plus swelling). **P*<0.05 vs WT, #*P*<0.05 vs untreated S218L HET after 60 minutes of fMCAO.

that mice expressing FHM1 mutations are particularly susceptible to infarction when challenged by cerebral arterial occlusion.

**Enhanced Neuroprotective Efficacy of Glutamate Receptor Antagonist MK-801.** FHM1 mutations enhance glutamate release,[11] and glutamate plays a pivotal role in spreading depression and ischemic depolarizations, as well as in excitotoxic cell death, mainly via the *N*-methyl-*D*-aspartate (NMDA) subtype of receptors. Therefore, we tested whether enhanced glutamatergic activity in FHM1 mutants is responsible for their vulnerability to infarction. Preischemic treatment with the NMDA receptor inhibitor MK-801 abolished the differences in stroke phenotype between genotypes. MK-801 reduced infarct volume by 45% in S218L HET compared with only 23% in WT (Figure 5A), and functional outcome was improved only in S218L mutants (Table 1).

As an important control, we also examined the density of glutamate and $GABA_A$ binding sites in the FHM1 mutant and WT mice using quantitative in vitro autoradiography and did not find overt differences (Supplemental Figure 3 and Supplemental Table 4). These data are consistent with recent proteomics analysis of cortical synapses in this mutant[31] and suggest that enhanced susceptibility to ischemic depolarizations in FHM1 mutants is unlikely to reflect changes in neurotransmitter receptors and reuptake mechanisms.

## DISCUSSION

Our data provide a novel mechanism to explain the higher incidence of ischemic stroke in migraineurs. Two genetic mouse models expressing FHM1 mutations were at risk of developing large infarcts and worse neurological outcomes after transient focal cerebral ischemia. Consistent with the higher stroke risk in women compared with men with migraine with aura, we found more striking increases in infarct volume in female mutants compared with males. Faster anoxic depolarization rates, more frequent PIDs, and enhanced neuroprotective efficacy of the NMDA antagonist MK-801 in the mutants implicated glutamatergic neuronal hyperexcitability as 1 mechanism, and larger perfusion defects linked to ischemic depolarizations implicated vasoconstrictive neurovascular coupling as another. Therefore, neuronal and vascular mechanisms together render migraineurs more vulnerable to cerebral infarction on ischemia.

The data have clinical implications. In susceptible migraineurs, increased sensitivity to ischemia may predispose to strokes during mild ischemic events, which remain clinically silent or manifest only as transient ischemic attacks in nonmigraineurs. Moreover, elevated CBF threshold for viability,[32] a sign of increased vulnerability to ischemia, may promote rapid infarct expansion into tissue with milder perfusion deficits, diminish salvageable tissue at risk (ie, ischemic penumbra), and shorten the therapeutic window of acute stroke interventions in migraineurs. Lastly, higher

mortality among the S218L mutants may have implications for malignant infarcts, large supratentorial strokes characterized by progressive loss of consciousness over 48 hours with up to 80% mortality if untreated.[33] To date, there has been no reliable predictor for malignant infarction, and history of migraine with aura (or its genetic determinants) may be 1 such marker increasing the risk of stroke progression and, in case of large territorial infarcts, the risk of death, as has recently been reported for hemorrhagic stroke in migraineurs.[34]

**Mechanisms of Ischemic Vulnerability in FHM1 Mice.** Biological mechanisms underlying the association between migraine and stroke are unknown, although in both diseases dynamic interactions among the constituents of the neurovascular unit are important to the pathophysiology. At the onset of cerebral ischemia, the gradual failure of $Na^+/K^+$-ATPase causes a slow rise in extracellular $K^+$ and loss of neuronal membrane potential until a critical threshold for initiation of anoxic depolarization is reached.[35,36] FHM1 mutations shift the $Ca_V2.1$ channel opening voltage to more negative membrane potentials so that channels open with smaller depolarizations, triggering glutamate release, which can explain faster anoxic depolarization onset in the mutants. Glutamate is also critical for PIDs, which are spreading depolarization waves triggered in ischemic penumbra. Therefore, enhanced release in ischemic penumbra can also explain higher PID frequencies in FHM1 mutants.[11] Delayed $Ca_V2.1$ channel inactivation may exacerbate the excitotoxicity by prolonging the $Ca^{2+}$ influx and glutamate release during PIDs in penumbra. Moreover, PIDs exacerbate the metabolic mismatch in penumbra by stimulating $O_2$ and glucose consumption and by worsening tissue perfusion via vasoconstrictive (ie, inverse) neurovascular coupling,[18,19,23] particularly when they occur with high frequency and in clusters, as observed in FHM1 mutants.[19,37-39] With each PID, more of the penumbra is incorporated into the core, accounting for concentric infarct growth over time.[22,40-42] PIDs occur frequently in human brain after ischemic or hemorrhagic stroke and head trauma and appear to worsen patient outcomes, similar to experimental stroke.[38,43-45] Hence, migraine with aura may be a risk factor for increased occurrence of PIDs and worse outcomes in human stroke, as recently suggested in subarachnoid hemorrhage.[46]

**Association Between Migraine and Stroke**. Our data in FHM1 mutant mice support shared genetic risk factors enhancing susceptibility to spreading depression as a mechanism to explain the migraine-stroke association. Shared genetic factors enhancing susceptibility to migraine and stroke such as *NOTCH3* mutations in cerebral autosomal dominant arteriopathy with subcortical infarcts and leukoencephalopathy have been described.[47-50] Indeed, *NOTCH3* mutations, despite being exclusively expressed in vascular smooth muscle cells, augment susceptibility to spreading depression.[51] Mutations associated with FHM2 and FHM3 are also predicted to

enhance neuronal excitability and spreading depression susceptibility possibly via glutamatergic mechanisms.[52] Glutamatergic mechanisms and hyperexcitability also are implicated in common forms of migraine by recent studies linking *AEG1*, encoding a regulator of glial glutamate transporter EAAT2, and *KCNK18*, encoding the TRESK potassium channel, to migraine.[15,16] Vascular mechanisms (eg, endothelial dysfunction) have also been implicated in increasing stroke risk in migraineurs.[53,54] Indeed, functional $Ca_v2.1$ channel expression has been reported in renovascular smooth muscle cells,[55,56] but whether FHM1 mutations alter cerebrovascular physiology is not known. Together with parenchymal mechanisms that enhance vulnerability to perfusion deficits, vascular mechanisms might further augment stroke risk in migraineurs. For example, highly focal and mild ischemic vascular events such as microembolism[57] may trigger spreading depression more readily in migraineurs highly susceptible to ischemic depolarizations, providing a possible explanation for the origin of a subset of migraine auras.

**Conclusions.** A monogenic determinant of migraine with aura increases stroke vulnerability via glutamatergic mechanisms that enhance susceptibility to ischemic depolarizations akin to spreading depression and accelerate stroke evolution. Hence, our data put FHM1 mutations among the shared genetic determinants of migraine with aura and stroke. More work is needed to extrapolate these data to other monogenic syndromes and to the more common and genetically more complex forms of migraine with aura and to determine whether targeting hyperexcitability and spreading depression such as migraine prophylaxis[58] confers ischemic protection in susceptible mouse strains or in migraineurs.

## ACKNOWLEDGMENTS

This work was supported by the American Heart Association (09GRNT2060416, 10SDG2610275); National Institutes of Health (NIH; NS061505, NS055104, NS35611, NS057556, DA024235, DA026108); Deane Institute for Integrative Research in Stroke and Atrial Fibrillation; Netherlands Organization for Scientific Research (903-52-291 and Vici 918.56.602; Spinoza 2009); EU EUROHEAD grant (LSHM-CT-2004-504837); Centre for Medical Systems Biology in the framework of the Netherlands Genomics Initiative; Basic Science Research Program through the National Research Foundation of Korea funded by the Ministry of Education, Science and Technology (2009-0066654); and Harvard Catalyst/The Harvard Clinical and Translational Science Center (NIH award UL1 RR 025758 and financial contributions from Harvard University and its affiliated academic healthcare centers).

## SUPPLEMENTARY MATERIAL

| | | N | Age (mo) | Weight (g) | BP (mmHg) | Arterial pH | Arterial $pCO_2$ (mmHg) | Arterial $pO_2$ (mmHg) |
|---|---|---|---|---|---|---|---|---|
| R192Q | WT | 11 | 3.8±0.2 | 27±1 | 84±2 | 7.36±0.01 | 33±1 | 147±4 |
| | HOM | 16 | 4.5±0.4 | 27±1 | 90±2 | 7.36±0.01 | 36±4 | 136±1 |
| S218L | WT | 23 | 4.4±0.2 | 27±1 | 89±3 | 7.36±0.01 | 37±1 | 129±12 |
| | HOM | 20 | 3.9±0.2 | 26±1 | 97±3 | 7.38±0.01 | 35±1 | 127±6 |

**Supplemental Table 1. Age, body weight and systemic physiological parameters.** There was no statistically significant difference between WT and HOM physiology was measured via a femoral artery catheter in non-survival experiments only, to minimize morbidity in survival groups.

| | WT | R192Q HOM | p |
|---|---|---|---|
| Cortex | 130 ± 28 | 130 ± 17 | 0.993 |
| Striatum | 139 ± 29 | 146 ± 16 | 0.649 |
| Cerebellum | 150 ± 24 | 162 ± 15 | 0.344 |

**Supplemental Table 2. Resting cerebral blood flow.** Values are absolute blood flow in ml/100g/min determined by [$^{14}$C]-iodoamphetamine radioactive tracer method. N=5 each genotype.

| | WT (n=7) | S218L HOM (n=7) | p |
|---|---|---|---|
| ICA diameter (μm) | 132 ± 5 | 128 ± 2 | 0.487 |
| MCA diameter (μm) | 111 ± 5 | 103 ± 3 | 0.230 |
| ACA diameter (μm) | 113 ± 5 | 105 ± 6 | 0.338 |
| PCA diameter (μm) | 115 ± 4 | 111 ± 2 | 0.391 |
| BA diameter (μm) | 163 ± 5 | 160 ± 7 | 0.707 |
| PComA diameter (μm) | 31 ± 3 | 29 ± 7 | 0.806 |
| Number of mice with unilaterally absent PComA (n) | 1 | 3 | 0.237 |
| Number of pial anastomoses between MCA and ACA (n) | 6.9 ± 0.9 | 6.6 ± 1.0 | 0.692 |
| Anastomoses distance from midline (mm) | | | |
| Rostral 1/3 of cortex | 1.6 ± 0.1 | 1.5 ± 0.1 | 0.235 |
| Middle 1/3 of cortex | 1.8 ± 0.1 | 1.9 ± 0.1 | 0.383 |
| Caudal 1/3 of cortex | 2.0 ± 0.1 | 2.1 ± 0.2 | 0.149 |

**Supplemental Table 3. Cerebrovascular anatomy.** Data were obtained using intracardiac carbon black infusion. Please also see Supplementary Figure 1 for representative images, abbreviations and the method of measurements.

| | EAAT | | AMPA | | KA | | NMDA | | $GABA_A$ | |
|---|---|---|---|---|---|---|---|---|---|---|
| $x10^{-3}$ | WT | R192Q HOM | WT | R192Q HOM | WT | R192Q HOM | WT | R192Q HOM | WT | R192Q HOM |
| Cortex | 85 ± 7 | 60 ± 5 | 279 ± 14 | 265 ± 20 | 157 ± 14 | 139 ± 7 | 204 ± 8 | 207 ± 4 | 145 ± 6 | 133 ± 9 |
| Striatum | 83 ± 6 | 75 ± 8 | 274 ± 18 | 271 ± 17 | 163 ± 11 | 146 ± 6 | 127 ± 9 | 128 ± 10 | 112 ± 6 | 98 ± 15 |
| Hippocampus | 134 ± 12 | 133 ± 13 | 691 ± 114 | 764 ± 95 | 94 ± 6 | 84 ± 5 | 429 ± 33 | 365 ± 20 | 127 ± 6 | 127 ± 10 |

**Supplemental Table 4. Quantitative receptor autoradiography.** Values indicate relative optical densities ($x10^{-3}$). Although ligand binding differed among regions, we did not detect a statistically significant effect of genotype on ligand binding within cortex (visual, somatosensory, and parietal cortex), hippocampus (CA1 region) and striatum (N=8 each). The ligands were: D-[2,3-$^3$H]Aspartic acid (GE Life Sciences, Piscataway, NJ) for, excitatory amino acid transporters (EAAT); DL-[5-methyl-$^3$H]-(AMPA) (Perkin-Elmer, Boston) for α-amino-3-Hydroxy-5-methylisoxazole-4-propionic acid (AMPA) ionotropic glutamate receptors; [$^3$H]Kainic Acid for ionotropic glutamate kainic acid receptors; [$^3$H]MK-801 (American Radiolabeled Chemicals, St-Louis, MO) for the N-methyl-D-aspartate (NMDA) subtype of ionotropic glutamate receptors; [$^3$H]muscimol (Perkin-Elmer, Boston) for ionotropic $GABA_A$ receptors.

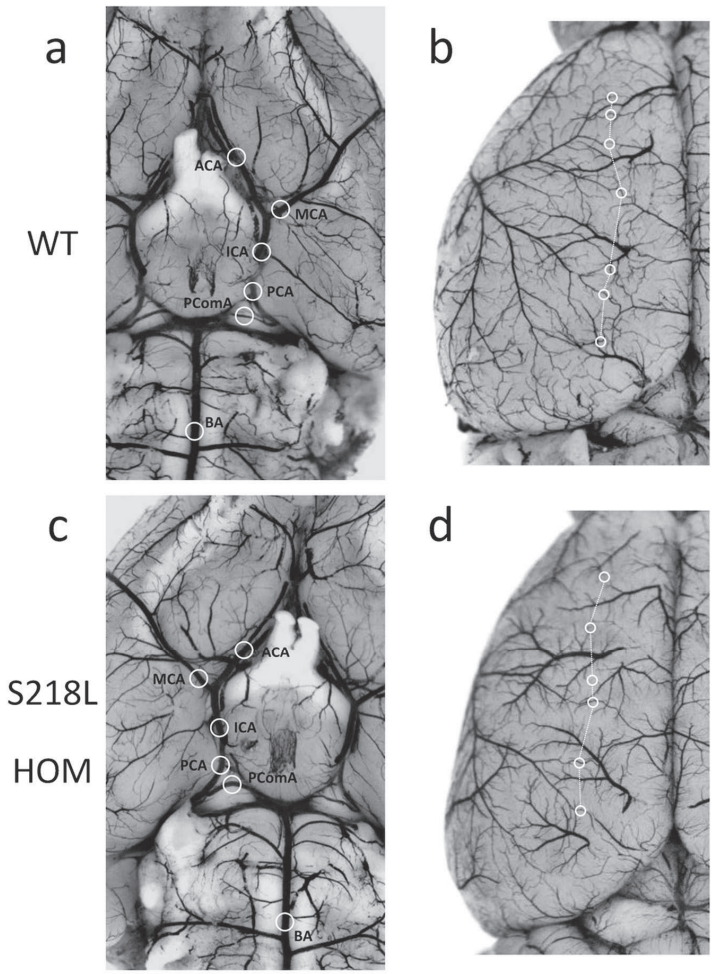


**Supplemental Figure 1. Normal cerebrovascular anatomy in FHM1 mutant mice.** Representative ventral (**A, C**) and dorsal (**B, D**) views of representative WT and S218L HOM brains show the circle of Willis anatomy, and pial arterial anastomoses between middle and anterior cerebral arteries, respectively, after transcardiac ink perfusion (1.4 ml, 0.5 ml/sec) under deep isoflurane anesthesia. Circles on the ventral surface (**A, C**) indicate where arterial diameters were measured, whereas circles on the dorsal surface (**B, D**) indicate the pial anatomoses (inset) that have been analyzed for their number and distance to midline. None of these endpoints significantly differed between WT and S218L HOM mice (Supplemental Table 3). Pial anastomoses were defined as the narrowest part of the vessel or half way between the nearest branch points of the anterior and the middle cerebral artery, localized by tracing the peripheral branches of these major vessels. ACA, anterior cerebral artery; MCA, middle cerebral artery; ICA, internal carotid artery; PCA, posterior cerebral artery; PComA, posterior communicating artery; BA, basilar artery.

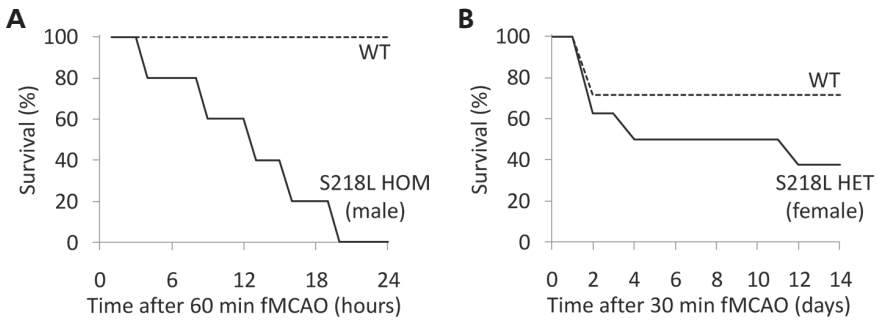


**Supplemental Figure 2. Increased mortality after stroke in FHM1 mutant mice.** Survival curves show the timing of mortality after filament middle cerebral artery occlusion (fMCAO). Mortality rate was (**A**) 100% and 0% within 24h after 60 min fMCAO in male S218L HOM and WT mice, respectively (n=5 and 4), and (**B**) 62% and 30% within 2 weeks after 30 min fMCAO in female S218L HET and WT mice, respectively (n=8 and 7).

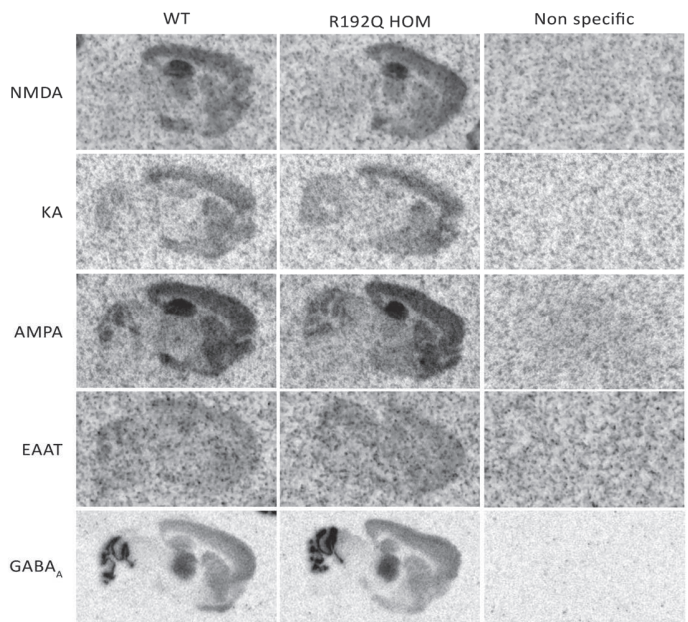


**Supplemental Figure 3. Normal density of Glutamate and GABAA binding sites in FHM1 mutant mice.** Representative autoradiograms on sagittal brain sections from WT and R192Q HOM mice showing specific binding for five commonly used ligands for ionotropic glutamate (N-methyl-D-aspartate, NMDA; α-amino-3-hydroxyl-5-methyl-4-isoxazole-propionate, AMPA; kainic acid, KA) and $GABA_A$ receptors and glutamate reuptake (EAAT) sites. Darker areas represent brain regions with higher levels of bound radioligand. Nonspecific binding, also shown, was not significantly different from background levels. Quantitative data are shown in Supplemental Table 4.

**Supplemental Movies**

*(http://circ.ahajournals.org/content/suppl/2011/12/05/CIRCULATIONAHA.111.045096.DC1)*

1. **Cerebral blood flow changes during distal MCAO in WT mice.** This representative movie of CBF shows the spatiotemporal hemodynamic changes upon distal MCAO by a microvascular clip through a temporal burr hole. Imaging field was positioned as shown in Figures 3 and 4 and imaging was performed through intact skull. Color bar shows CBF as % of pre-ischemic baseline. Time after imaging onset is shown on the top. MCA is clipped between 1 and 2 min (clip artifact visible in the lower right of the imaging field). Approximately 1-2 min after clipping, a wave of further decrease in perfusion originates from ischemic core and spreads throughout the ipsilateral hemisphere; this wave has previously been shown to correspond to anoxic depolarization. During the 60 min dMCAO, 1 distinct wave of spreading hypoperfusion is spontaneously triggered in the WT; this hypoperfusion transient corresponds to a peri-infarct depolarization. Reperfusion is achieved by removing the clip approximately 60 min after the onset of ischemia.
2. **Cerebral blood flow changes during distal MCAO in S218L HOM mutant mice.** This representative movie of CBF shows the spatiotemporal hemodynamic changes upon distal MCAO by a microvascular clip through a temporal burr hole, in S218L HOM mutant mice. Please see legend to Movie 1 for imaging details. During the 60 min dMCAO, 8 distinct waves of spreading hypoperfusion events are spontaneously triggered in the S218L HOM mutant; these hypoperfusion transients correspond to peri-infarct depolarizations and cause a lasting decrease in tissue perfusion in their wake.

## REFERENCES


1. Etminan M, Takkouche B, Isorna FC, Samii A. 2005. Risk of ischaemic stroke in people with migraine: systematic review and meta-analysis of observational studies. *BMJ*. 330:63.
2. Schurks M, Rist PM, Bigal ME, Buring JE, Lipton RB, Kurth T. 2009. Migraine and cardiovascular disease: systematic review and meta-analysis. *BMJ*. 339:b3914.
3. Kruit MC, van Buchem MA, Hofman PA, Bakkers JT, Terwindt GM, Ferrari MD, Launer LJ. 2004. Migraine as a risk factor for subclinical brain lesions. *JAMA*. 291:427-434.
4. Scher AI, Gudmundsson LS, Sigurdsson S, Ghambaryan A, Aspelund T, Eiriksdottir G, van Buchem MA, Gudnason V, Launer LJ. 2009. Migraine headache in middle age and late-life brain infarcts. *JAMA*. 301: 2563-2570.
5. Thomsen LL, Eriksen MK, Roemer SF, Andersen I, Olesen J, Russell MB. 2002. A population-based study of familial hemiplegic migraine suggests revised diagnostic criteria. *Brain*. 125:1379-1391.
6. Terwindt GM, Ophoff RA, Haan J, Vergouwe MN, van Eijk R, Frants RR, Ferrari MD. 1998. Variable clinical expression of mutations in the p/q-type calcium channel gene in familial hemiplegic migraine: Dutch Migraine Genetics Research Group. *Neurology*. 50:1105-1110.
7. Ducros A, Denier C, Joutel A, Cecillon M, Lescoat C, Vahedi K, Darcel F, Vicaut E, Bousser MG, Tournier-Lasserve E. 2001. The clinical spectrum of familial hemiplegic migraine associated with mutations in a neuronal calcium channel. *N Engl J Med*. 345:17-24.
8. Moskowitz MA, Bolay H, Dalkara T. 2004. Deciphering migraine mechanisms: clues from familial hemiplegic migraine genotypes. *Ann Neurol*. 55:276-280.
9. Ophoff RA, Terwindt GM, Vergouwe MN, van Eijk R, Oefner PJ, Hoffman SM, Lamerdin JE, Mohrenweiser HW, Bulman DE, Ferrari M, Haan J, Lindhout D, van Ommen GJ, Hofker MH, Ferrari MD, Frants RR. 1996. Familial hemiplegic migraine and episodic ataxia type-2 are caused by mutations in the Ca2+ channel gene CACNL1A4. *Cell*. 87:543-552.
10. Tottene A, Pivotto F, Fellin T, Cesetti T, van den Maagdenberg AM, Pietrobon D. 2005. Specific kinetic alterations of human CaV2.1 calcium channels produced by mutation S218L causing familial hemiplegic migraine and delayed cerebral edema and coma after minor head trauma. *J Biol Chem*. 280:17678-17686.
11. Tottene A, Conti R, Fabbro A, Vecchia D, Shapovalova M, Santello M, van den Maagdenberg AM, Ferrari MD, Pietrobon D. 2009. Enhanced excitatory transmission at cortical synapses as the basis for facilitated spreading depression in Ca (v) 2.1 knockin migraine mice. *Neuron*. 61:762-773.
12. van den Maagdenberg AM, Pizzorusso T, Kaja S, Terpolilli N, Shapovalova M, Hoebeek FE, Barrett CF, Gherardini L, van de Ven RC, Todorov B, Broos LA, Tottene A, Gao Z, Fodor M, De Zeeuw CI, Frants RR, Plesnila N, Plomp JJ, Pietrobon D, Ferrari MD. 2010. High cortical spreading depression susceptibility and migraine-associated symptoms in Ca(v)2.1 S218L mice. *Ann Neurol*. 67:85–98.
13. Eikermann-Haerter K, Dilekoz E, Kudo C, Savitz SI, Waeber C, Baum MJ, Ferrari MD, van den Maagdenberg AM, Moskowitz MA, Ayata C. 2009. Genetic and hormonal factors modulate spreading depression and transient hemiparesis in mouse models of familial hemiplegic migraine type 1. *J Clin Invest*. 119:99-109.
14. van den Maagdenberg AM, Pietrobon D, Pizzorusso T, Kaja S, Broos LA, Cesetti T, van de Ven RC, Tottene A, van der Kaa J, Plomp JJ, Frants RR, Ferrari MD. 2004. A cacna1a knockin migraine mouse model with increased susceptibility to cortical spreading depression. *Neuron*. 41:701-710.
15. Lafreniere RG, Cader MZ, Poulin JF, Andres-Enguix I, Simoneau M, Gupta N, Boisvert K, Lafreniere F, McLaughlan S, Dube MP, Marcinkiewicz MM, Ramagopalan S, Ansorge O, Brais B, Sequeiros J, Pereira-Monteiro JM, Griffiths LR, Tucker SJ, Ebers G, Rouleau GA. 2011. A dominant-negative mutation in the TRESK potassium channel is linked to familial migraine with aura. *Nat Med*. 16:1157-1160.

16. Anttila V, Stefansson H, Kallela M, Todt U, Terwindt GM, Calafato MS, Nyholt DR, Dimas AS, Freilinger T, Muller-Myhsok B, Artto V, Inouye M, Alakurtti K, Kaunisto MA, Hamalainen E, de Vries B, Stam AH, Weller CM, Heinze A, Heinze-Kuhn K, Goebel I, Borck G, Gobel H, Steinberg S, Wolf C, Bjornsson A, Gudmundsson G, Kirchmann M, Hauge A, Werge T, Schoenen J, Eriksson JG, Hagen K, Stovner L, Wichmann HE, Meitinger T, Alexander M, Moebus S, Schreiber S, Aulchenko YS, Breteler MM, Uitterlinden AG, Hofman A, van Duijn CM, Tikka-Kleemola P, Vepsalainen S, Lucae S, Tozzi F, Muglia P, Barrett J, Kaprio J, Farkkila M, Peltonen L, Stefansson K, Zwart JA, Ferrari MD, Olesen J, Daly M, Wessman M, van den Maagdenberg AM, Dichgans M, Kubisch C, Dermitzakis ET, Frants RR, Palotie A. 2011. Genome-wide association study of migraine implicates a common susceptibility variant on 8q22.1. *Nat Genet*. 42:869-873.
17. Ayata C, Ayata G, Hara H, Matthews RT, Beal MF, Ferrante RJ, Endres M, Kim A, Christie RH, Waeber C, Huang PL, Hyman BT, Moskowitz MA. 1997. Mechanisms of reduced striatal NMDA excitotoxicity in type I nitric oxide synthase knock-out mice. *J Neurosci*. 17:6908-6917.
18. Shin HK, Dunn AK, Jones PB, Boas DA, Moskowitz MA, Ayata C. 2006. Vasoconstrictive neurovascular coupling during focal ischemic depolarizations. *J Cereb Blood Flow Metab*. 26:1018-1030.
19. Strong AJ, Anderson PJ, Watts HR, Virley DJ, Lloyd A, Irving EA, Nagafuji T, Ninomiya M, Nakamura H, Dunn AK, Graf R. 2007. Peri-infarct depolarizations lead to loss of perfusion in ischaemic gyrencephalic cerebral cortex. *Brain*. 130:995-1008.
20. Hartings JA, Rolli ML, Lu XC, Tortella FC. 2003. Delayed secondary phase of peri-infarct depolarizations after focal cerebral ischemia: relation to infarct growth and neuroprotection. *J Neurosci*. 23:11602-11610.
21. Hopwood SE, Parkin MC, Bezzina EL, Boutelle MG, Strong AJ. 2005. Transient changes in cortical glucose and lactate levels associated with peri-infarct depolarisations, studied with rapid-sampling microdialysis. *J Cereb Blood Flow Metab*. 25:391-401.
22. Nakamura H, Strong AJ, Dohmen C, Sakowitz OW, Vollmar S, Sue M, Kracht L, Hashemi P, Bhatia R, Yoshimine T, Dreier JP, Dunn AK, Graf R. 2010. Spreading depolarizations cycle around and enlarge focal ischaemic brain lesions. *Brain*. 133:1994-2006.
23. Dreier JP, Windmüller O, Petzold G, Lindauer U, Einhäupl KM, Dirnagl U. 2002. Ischemia caused by inverse coupling between neuronal activation and cerebral blood flow in rats. In: Tomita M, Kanno I, Hamel E, eds. *Brain Activation and CBF Control* Amsterdam, Netherlands: Elsevier; 487-492.
24. Shin HK, Jones PB, Garcia-Alloza M, Borrelli L, Greenberg SM, Bacskai BJ, Frosch MP, Hyman BT, Moskowitz MA, Ayata C. 2007. Age-dependent cerebrovascular dysfunction in a transgenic mouse model of cerebral amyloid angiopathy. *Brain*. 130:2310-2319.
25. Ayata C, Dunn AK, Gursoy OY, Huang Z, Boas DA, Moskowitz MA. 2004. Laser speckle flowmetry for the study of cerebrovascular physiology in normal and ischemic mouse cortex. *J Cereb Blood Flow Metab*. 24:744-755.
26. Rasmussen BK, Jensen R, Schroll M, Olesen J. 1991. Epidemiology of headache in a general population: a prevalence study. *J Clin Epidemiol*. 44:1147-1157.
27. Bille BS. 1962. Migraine in school children: a study of the incidence and short-term prognosis, and a clinical, psychological and electroencephalographic comparison between children with migraine and matched controls. *Acta Paediatr*. 136:1-151.
28. Eriksen MK, Thomsen LL, Olesen J. 2006. Implications of clinical subtypes of migraine with aura. *Headache*. 46:286-297.
29. Thomsen LL, Kirchmann M, Bjornsson A, Stefansson H, Jensen RM, Fasquel AC, Petursson H, Stefansson M, Frigge ML, Kong A, Gulcher J, Stefansson K, Olesen J. 2007. The genetic spectrum of a population-based sample of familial hemiplegic migraine. *Brain*. 130:346-356.

30. Eikermann-Haerter K, Baum MJ, Ferrari MD, van den Maagdenberg AM, Moskowitz MA, Ayata C. 2009. Androgenic suppression of spreading depression in familial hemiplegic migraine type 1 mutant mice. *Ann Neurol*. 66:564-568.
31. Klychnikov OI, Li KW, Sidorov IA, Loos M, Spijker S, Broos LA, Frants RR, Ferrari MD, Mayboroda OA, Deelder AM, Smit AB, van den Maagdenberg AM. 2010. Quantitative cortical synapse proteomics of a transgenic migraine mouse model with mutated Ca (v) 2.1 calcium channels. *Proteomics*. 10:2531-2535.
32. Astrup J, Siesjo BK, Symon L. 1981. Thresholds in cerebral ischemia: the ischemic penumbra. *Stroke*. 12:723-725.
33. Huttner HB, Schwab S. 2009. Malignant middle cerebral artery infarction: clinical characteristics, treatment strategies, and future perspectives. *Lancet Neurol*. 8:949-958.
34. Kurth T, Kase CS, Schurks M, Tzourio C, Buring JE. 2010. Migraine and risk of haemorrhagic stroke in women: prospective study. *BMJ*. 341: c3659.
35. Vyskocil F, Kritz N, Bures J. 1972. Potassium-selective microelectrodes used for measuring the extracellular brain potassium during spreading depression and anoxic depolarization in rats. *Brain Res*. 39: 255-259.
36. Astrup J, Symon L, Branston NM, Lassen NA. 1977. Cortical evoked potential and extracellular K+ and H+ at critical levels of brain ischemia. *Stroke*. 8:51-57.
37. Dreier JP, Woitzik J, Fabricius M, Bhatia R, Major S, Drenckhahn C, Lehmann TN, Sarrafzadeh A, Willumsen L, Hartings JA, Sakowitz OW, Seemann JH, Thieme A, Lauritzen M, Strong AJ. 2006. Delayed ischaemic neurological deficits after subarachnoid haemorrhage are associated with clusters of spreading depolarizations. *Brain*. 129:3224-3237.
38. Dohmen C, Sakowitz OW, Fabricius M, Bosche B, Reithmeier T, Ernestus RI, Brinker G, Dreier JP, Woitzik J, Strong AJ, Graf R. 2008. Spreading depolarizations occur in human ischemic stroke with high incidence. *Ann Neurol*. 63:720-728.
39. Back T, Kohno K, Hossmann KA. 1994. Cortical negative dc deflections following middle cerebral artery occlusion and KCl-induced spreading depression: effect on blood flow, tissue oxygenation, and electroencephalogram. *J Cereb Blood Flow Metab*. 14:12-19.
40. Higuchi T, Takeda Y, Hashimoto M, Nagano O, Hirakawa M. 2002. Dynamic changes in cortical NADH fluorescence and direct current potential in rat focal ischemia: relationship between propagation of recurrent depolarization and growth of the ischemic core. *J Cereb Blood Flow Metab*. 22:71-79.
41. Busch E, Gyngell ML, Eis M, Hoehn-Berlage M, Hossmann KA. 1996. Potassium-induced cortical spreading depressions during focal cerebral ischemia in rats: Contribution to lesion growth assessed by diffusion-weighted NMR and biochemical imaging. *J Cereb Blood Flow Metab*. 16:1090-1099.
42. Takano K, Latour LL, Formato JE, Carano RA, Helmer KG, Hasegawa Y, Sotak CH, Fisher M. 1996. The role of spreading depression in focal ischemia evaluated by diffusion mapping. *Ann Neurol*. 39:308 –318.
43. Strong AJ, Hartings JA, Dreier JP. 2007. Cortical spreading depression: an adverse but treatable factor in intensive care? *Curr Opin Crit Care*. 13:126-133.
44. Dreier JP, Major S, Manning A, Woitzik J, Drenckhahn C, Steinbrink J, Tolias C, Oliveira-Ferreira AI, Fabricius M, Hartings JA, Vajkoczy P, Lauritzen M, Dirnagl U, Bohner G, Strong AJ. 2009. Cortical spreading ischaemia is a novel process involved in ischaemic damage in patients with aneurysmal subarachnoid haemorrhage. *Brain*. 132:1866-1881.
45. Bosche B, Graf R, Ernestus RI, Dohmen C, Reithmeier T, Brinker G, Strong AJ, Dreier JP, Woitzik J. 2010. Recurrent spreading depolarizations after subarachnoid hemorrhage decreases oxygen availability in human cerebral cortex. *Ann Neurol*. 67:607-617.

46. Dreier JP, Kremer C, Lammers G, Lohmann F, Hansen HC, Valdueza JM. 2007. Migraine and delayed ischaemic neurological deficit after subarachnoid haemorrhage in women: a case-control study. *Eur J Neurol*. 14:1363-1368.
47. Scher AI, Terwindt GM, Verschuren WM, Kruit MC, Blom HJ, Kowa H, Frants RR, van den Maagdenberg AM, van Buchem M, Ferrari MD, Launer LJ. 2006. Migraine and MTHFR c677t genotype in a population-based sample. *Ann Neurol*. 59:372-375.
48. Stam AH, Haan J, van den Maagdenberg AM, Ferrari MD, Terwindt GM. 2009. Migraine and genetic and acquired vasculopathies. *Cephalalgia*. 29:1006-1017.
49. Pezzini A, Grassi M, Del Zotto E, Giossi A, Monastero R, Dalla Volta G, Archetti S, Zavarise P, Camarda C, Gasparotti R, Magoni M, Camarda R, Padovani A. 2007. Migraine mediates the influence of c677t MTHFR genotypes on ischemic stroke risk with a stroke-subtype effect. *Stroke*. 38: 3145-3151.
50. Schurks M, Zee RY, Buring JE, Kurth T. 2008. Interrelationships among the MTHFR 677C T polymorphism, migraine, and cardiovascular disease. *Neurology*. 71:505-513.
51. Eikermann-Haerter K, Yuzawa I, Dilekoz E, Joutel A, Moskowitz MA, Ayata C. 2011. Cerebral autosomal dominant arteriopathy with subcortical infarcts and leukoencephalopathy syndrome mutations increase susceptibility to spreading depression. *Ann Neurol*. 69:413-418.
52. van den Maagdenberg AM, Haan J, Terwindt GM, Ferrari MD. 2007. Migraine: gene mutations and functional consequences. *Curr Opin Neurol*. 20:299-305.
53. Tietjen EG. 2007. Migraine and ischaemic heart disease and stroke: potential mechanisms and treatment implications. *Cephalalgia*. 27: 981-987.
54. Bigal ME, Kurth T, Hu H, Santanello N, Lipton RB. 2009. Migraine and cardiovascular disease: possible mechanisms of interaction. *Neurology*. 72:1864-1871.
55. Hansen PB, Poulsen CB, Walter S, Marcussen N, Cribbs LL, Skott O, Jensen BL. 2011. Functional importance of L- and P/Q-type voltage-gated calcium channels in human renal vasculature. *Hypertension*. 58:464-470.
56. Hansen PB, Jensen BL, Andreasen D, Friis UG, Skott O. 2000. Vascular smooth muscle cells express the alpha(1a) subunit of a P-/Q-type voltage-dependent Ca(2+)channel, and it is functionally important in renal afferent arterioles. *Circ Res*. 87:896-902.
57. Nozari A, Dilekoz E, Sukhotinsky I, Stein T, Eikermann-Haerter K, Liu C, Wang Y, Frosch MP, Waeber C, Ayata C, Moskowitz MA. 2010. Microemboli may link spreading depression, migraine aura, and patent foramen ovale. *Ann Neurol*. 67:221-229.
58. Ayata C, Jin H, Kudo C, Dalkara T, Moskowitz MA. 2006. Suppression of cortical spreading depression in migraine prophylaxis. *Ann Neurol*. 59:652-661.